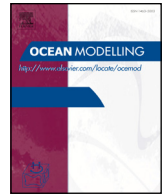




ELSEVIER

Contents lists available at ScienceDirect

Ocean Modelling

journal homepage: www.elsevier.com/locate/ocemod

Virtual Special Issue Ocean Surface Waves

On the modeling of wave-enhanced turbulence nearshore

Saeed Moghimi^{a,*}, Jim Thomson^b, Tuba Özkan-Haller^a, Lars Umlauf^c, Seth Zippel^b^a College of Earth, Ocean, and Atmospheric Sciences, Oregon State University, Corvallis, USA^b Applied Physics Laboratory, University of Washington, Seattle, USA^c Department of Physical Oceanography, Leibniz Institute for Baltic Sea Research, Warnemünde, Germany

ARTICLE INFO

Article history:

Received 17 February 2015

Revised 9 September 2015

Accepted 1 November 2015

Available online 10 November 2015

Keywords:

Turbulence modeling

Wave modeling

Turbulence dissipation rate

One-dimensional vertical

Wave–current interaction

Wave–ocean energy exchange

ABSTRACT

A high resolution $k-\omega$ two-equation turbulence closure model, including surface wave forcing was employed to fully resolve turbulence dissipation rate profiles close to the ocean surface. Model results were compared with observations from Surface Wave Instrument Floats with Tracking (SWIFTs) in the nearshore region at New River Inlet, North Carolina USA, in June 2012. A sensitivity analysis for different physical parameters and wave and turbulence formulations was performed. The flux of turbulent kinetic energy (TKE) prescribed by wave dissipation from a numerical wave model was compared with the conventional prescription using the wind friction velocity. A surface roughness length of 0.6 times the significant wave height was proposed, and the flux of TKE was applied at a distance below the mean sea surface that is half of this roughness length. The wave enhanced layer had a total depth that is almost three times the significant wave height. In this layer the non-dimensionalized Terray scaling with power of -1.8 (instead of -2) was applicable.

© 2015 Elsevier Ltd. All rights reserved.

1. Introduction

Growing interest in fully coupled three-dimensional (3D) atmosphere–wave–ocean modeling systems motivates improvements to parameterizations and coupling between model components. Debate continues on whether momentum exchange between surface waves and the ocean circulation should be treated as a vortex force or radiation stress (Mellor, 2003; McWilliams et al., 2004; Ardhuin et al., 2008; Aiki and Greatbatch, 2014; Mellor, 2015). Similarly in recent years, the treatment of energy exchange between waves and ocean has been the subject of several research activities. A recent modeling study by Gerbi et al. (2013) shows the effects of white-capping dissipation on a river plume during an upwelling favorable wind condition using a three-dimensional coastal ocean model. Carniel et al. (2009) compare two-equation turbulence closure models to investigate the effects of surface wave breaking on surface drifter trajectory in the Adriatic Sea. However, in both of these studies, the effects of the momentum exchange between waves and ocean were not included.

Most modeling studies on surface wave breaking effects on turbulence and mixing quantities were conducted using a one-dimensional vertical (1DV) water column model following Craig and Banner (1994). They suggest a turbulent kinetic energy (TKE) balance between diffusion and dissipation, where the surface flux of TKE (associated with breaking waves) is prescribed as proportional to the surface wind friction velocity cubed (e.g. Burchard, 2001; Umlauf and Burchard, 2003; Umlauf et al., 2003; Kantha and Clayson, 2004). Raschle et al. (2013) utilized a 1DV Mellor and Yamada (1982) turbulence model to compare three different methods for simulating turbulence induced by surface breaking waves.

Most of the research on wave breaking turbulence and water column mixing are focused on the deep ocean and lakes. There have been some attempts to investigate these phenomenon in nearshore regions ($3 \text{ [m]} < \text{depth} < 10 \text{ [m]}$), surf-zones and shallow estuaries (e.g. Feddersen and Trowbridge, 2005; Feddersen, 2012b; Grasso et al., 2012; Jones and Monismith, 2008b). Feddersen and Trowbridge (2005) present a 1DV model, including a two-equation $k-\epsilon$ turbulence closure model, to study the effects of wave breaking turbulence on the mean circulation and turbulence quantities inside the surf-zone. Feddersen et al. (2007) extend their previous investigation from the surf-zone to the nearshore (outer surf-zone) region (depth $> 3 \text{ [m]}$). They use bottom mounted turbulence measurements to show that, to correctly estimate the vertical distribution of the TKE

* Corresponding author. Tel.: +1 541 737 3402; fax: +1 541 737 2064.

E-mail address: moghimi@coas.oregonstate.edu, moghimis@gmail.com (S. Moghimi).

dissipation rate according to Terray et al. (1996), a greater surface flux of energy is needed compared to the open ocean.

In this study, we used nearshore measurements of surface TKE dissipation rates from Surface Wave Instrumentation Floats with Tracking (SWIFT) buoys (Thomson, 2012) to investigate energy transfer from breaking waves to the ocean water column in the vicinity of a tidal inlet. Drawing on the modeling studies in similarly complex nearshore settings (e.g. Newberger and Allen, 2007; Kumar et al., 2012), we utilized coupled wave and circulation models to characterize the spatial variability of the wave and circulation field at the site. The wave and circulation models are coupled in a rudimentary fashion such that the effects of the tidal circulation on the wave kinematics and dynamics are included, resulting in a reasonable view of spatially varying wave field. Using this representation of the wave field, we then focused our attention on the effects of wave motions on water column turbulence properties. For this purpose we locally employed a high resolution, two-equation turbulence model of the ocean water column (with several hundred vertical layers) to fully resolve the TKE dissipation rate close to the water surface. We performed a wide range of sensitivity analyses to gain insight into the different physical parameters involved in the modeling procedure (e.g. surface roughness). Traditionally, following Craig and Banner (1994), the wind friction velocity is used in prescribing the surface boundary flux of TKE. However, it may be more reasonable to use the wave dissipation computed directly by a wave model instead of an approximation based on wind friction velocity. In this study, we compared two widely used methods for computing these wave related quantities and discussed their impact on the calculation of a TKE dissipation rate.

The structure of this paper is as follows. In Section 2, a brief description of the momentum and energy exchange between wind, waves and ocean is given, and the theoretical background and basic definition of parameters for the numerical experiments are discussed. The case study, the modeling system and observational data are described in Section 3. Modeling results of turbulence quantities and comparison with observational data are shown in Section 4. A more comprehensive discussion about the role of different parameters is presented in Section 5. Finally, the summary and conclusion of this research are described in Section 6.

2. Theory

Understanding and correctly parameterizing the exchange of momentum and energy between wind, waves and ocean are key to reasonably simulating the near surface region. Here, our focus is on the effect of surface wave breaking on turbulence quantities in the water column. We simulate the wave field using a common nearshore wave propagation model. Here, we assume wind as the main source of ocean surface momentum. A fraction of the wind momentum is consumed to generate local surface waves.

2.1. Wave modeling

The surface wave field evolution is described assuming that the waves can be described by irrotational inviscid linear wave theory. Clearly, breaking waves in the nearshore zone are not linear, the motions in the active breaking region are not irrotational, and waves can be dissipated by inviscid effects. However, the above assumptions are frequently employed with surprisingly successful results for wave prediction in the nearshore and surf-zones (e.g. Ruessink et al., 2001; Newberger and Allen, 2007) and the use of a simplified theory allows for progress over the complex domain of a tidal inlet. Further, we will show that the prediction of local wave quantities is skilled compared to observations. Nonetheless, as a result of the irrotational and inviscid assumptions, the detailed dynamics of air-sea energy exchange are not accounted for herein, instead we focus on the fate of the TKE provided to the water column by breaking wave events.

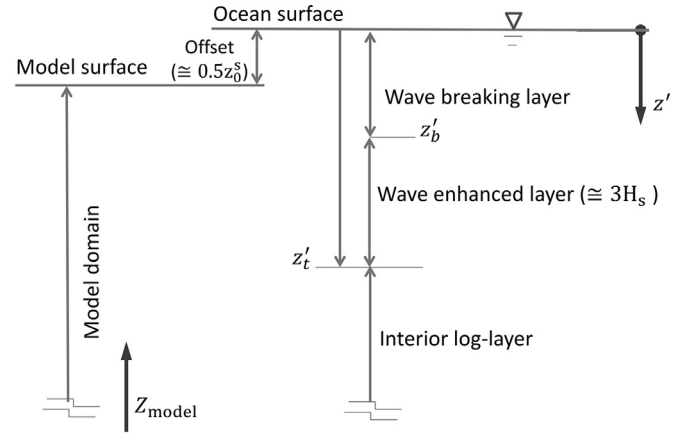


Fig. 1. Simplified schematic description of water column surface layers affected by breaking waves. Here H_s and z_0^s are the significant wave height and the surface roughness (see Section 2.2.1).

The governing equation for wave action balance (Komen et al., 1994), $\mathcal{N} = E(\omega_{\text{wave}}, \theta) / \omega_{\text{wave}}$, then reads:

$$\frac{\partial \mathcal{N}}{\partial t} + \nabla_{\mathbf{x}} \cdot [(\mathbf{c}_g + \mathbf{U})\mathcal{N}] + \frac{\partial (c_{\omega_{\text{wave}}}\mathcal{N})}{\partial \omega_{\text{wave}}} + \frac{\partial (c_{\theta}\mathcal{N})}{\partial \theta} = \frac{S^{\text{tot}}}{\omega_{\text{wave}}} \quad (1)$$

where E is the wave energy at relative angular frequency ω_{wave} traveling at an angle of θ , \mathbf{c}_g is the intrinsic wave group velocity vector, \mathbf{U} is ambient current velocity vector and \mathbf{X} is the horizontal geographic coordinate system. The propagation velocities in spectral space ($\omega_{\text{wave}}, \theta$) are given by $c_{\omega_{\text{wave}}}$ and c_{θ} . The terms on the left hand side of the equation are responsible for local changes and propagation of the wave energy. The right hand side of the equation represents source and sink terms associated with wave generation, dissipation and nonlinear wave-wave interactions, where:

$$S^{\text{tot}} = S^{\text{in}} + S^{\text{nl}} + S^{\text{ds,w}} + S^{\text{ds,br}} + S^{\text{ds,b}}. \quad (2)$$

S^{in} is the energy input from wind to the wave field, S^{nl} is the nonlinear wave-wave interaction, $S^{\text{ds,b}}$ is the dissipation due to bottom friction, $S^{\text{ds,br}}$ is the dissipation due to depth-induced surface wave breaking, and $S^{\text{ds,w}}$ is the dissipation due to white-capping.

2.2. Wave-enhanced turbulence

Surface breaking waves enhance the turbulence in the ocean surface layer by acting as a source of turbulence kinetic energy (TKE) (Kitaigorodskii et al., 1983; Thorpe, 1984). A one-dimensional vertical Mellor and Yamada (1982) turbulence closure model was adapted by Craig and Banner (1994) to account for wave-affected near surface turbulence. They suggested that the surface boundary condition for turbulent kinetic energy, k , could be approximated by a flux boundary condition:

$$F_k^s = -\frac{\nu_{\text{turb}}}{\sigma_k} \frac{\partial k}{\partial z}, \quad (3)$$

in which F_k^s is the flux of energy injected to the surface of the ocean due to surface wave dissipation (Section 2.2.1). Here ν_{turb} is the vertical eddy viscosity and σ_k is the turbulence Schmidt number (Mellor and Yamada, 1982). z is the positive upward vertical coordinate with $z = h$ at the surface and $z = 0$ at the bottom.

As shown in Fig. 1, the breaking layer is the closest layer to the mean sea surface where the direct injection of the turbulence and bubbles from surface breaking waves is taking place (from surface to depth of z'_b). Here z' is depth below mean sea surface. In the wave-enhanced layer, the effects of the turbulence injected by waves on the mixing properties of water column should be detected. Inside this layer, a balance between downward diffusion of the dissipated

energy from surface waves and turbulence dissipation is assumed. At its lower boundary, the wave-enhanced layer smoothly merges into the near-surface logarithmic boundary layer, where turbulence shear-production balances dissipation (Umlauf and Burchard, 2003). The offset between the position of model surface and the mean sea surface will be defined later as a fraction of significant wave height (see Section 5.1).

Subsequently, Umlauf and Burchard (2003) introduced a “generic length” scale two-equation turbulence closure model which compared favorably to the observed spatial decay rates for grid-generated turbulence that is often considered a simple representation of the wave-breaking problem. They also showed a similar behavior of the k - ω and their generic length scale models for this kind of application where ω is the inverse turbulence time scale or turbulent “frequency”. They suggested that, for scenarios with turbulence injection at the surface due to surface wave breaking, the k - ω model performed better than the k - ϵ model where ϵ is the turbulence dissipation rate. In addition, they illustrated that the k - ϵ model showed less depth of penetration with the same boundary condition and constant parameters in comparison to the k - ω model. Jones and Monismith (2008b) and Moghimi et al. (2013) also successfully applied the k - ω two-equation turbulence model in shallow tidal and barred beach environments. For the present study a k - ω turbulence closure model was also chosen.

2.2.1. Governing equations for wave-averaged quantities

The wave modified (low-pass time-filtered) momentum equations for Eulerian mean current velocities (u , v ; McWilliams et al., 1997), the averaged potential temperature T , the averaged salinity S , TKE k and ω (Wilcox, 1988; Umlauf et al., 2003), are given as:

$$\frac{\partial u}{\partial t} - \frac{\partial}{\partial z} \left((v + v_{\text{turb}}) \frac{\partial u}{\partial z} \right) = -\frac{1}{\rho_0} \frac{\partial p}{\partial x} + f(v + v_s) + F_x^{\text{Out, wave}}, \quad (4)$$

$$\frac{\partial v}{\partial t} - \frac{\partial}{\partial z} \left((v + v_{\text{turb}}) \frac{\partial v}{\partial z} \right) = -\frac{1}{\rho_0} \frac{\partial p}{\partial y} - f(u + u_s) + F_y^{\text{Out, wave}}, \quad (5)$$

$$\frac{\partial T}{\partial t} - \frac{\partial}{\partial z} \left((v' + v'_{\text{turb}}) \frac{\partial T}{\partial z} \right) = \frac{1}{C_p \rho_0} \frac{\partial I}{\partial z}, \quad (6)$$

$$\frac{\partial S}{\partial t} - \frac{\partial}{\partial z} \left((v'' + v''_{\text{turb}}) \frac{\partial S}{\partial z} \right) = 0, \quad (7)$$

$$\frac{\partial k}{\partial t} - \frac{\partial}{\partial z} \left(v_{\text{turb}} \frac{\partial k}{\partial z} \right) = \overbrace{v_{\text{turb}} \left(\left(\frac{\partial u}{\partial z} \right)^2 + \left(\frac{\partial v}{\partial z} \right)^2 \right)}^p + v'_{\text{turb}} \left(\frac{g}{\rho_0} \right) \frac{\partial \rho}{\partial z} - \epsilon, \quad (8)$$

$$\frac{\partial \omega}{\partial t} = \frac{\partial}{\partial z} \left(v_{\text{turb}} \frac{\partial \omega}{\partial z} \right) + \frac{\omega}{k} \left(c_{\omega 1} v_{\text{turb}} \left(\left(\frac{\partial u}{\partial z} \right)^2 + \left(\frac{\partial v}{\partial z} \right)^2 \right) + c_{\omega 3} v'_{\text{turb}} \left(\frac{g}{\rho_0} \right) \frac{\partial \rho}{\partial z} - c_{\omega 2} \epsilon \right) \quad (9)$$

where t is time, ρ is averaged density, $f = 2\omega_e \sin(\phi)$ with the Earth rotation's angular velocity ω_e and latitude ϕ , where, $u = u_L - u_s$, $v = v_L - v_s$ are defined as (quasi-)Eulerian velocities (Jenkins, 1987; 1989; Tang et al., 2007). u_L and v_L are Lagrangian mean velocities, u_s and v_s are surface wave Stokes drift velocities and, x and y are the horizontal coordinates.

In our approach, the model surface layer is situated some distance below the mean sea surface away from the layers most

affected by breaking events (see Fig. 14). Note that this approximation is more conservative than most of the wave-circulation coupling studies, particularly those that involved similar boundary conditions applied at the mean sea surface inside the surf-zone where a substantial portion of the water column is considered to be inside the active wave breaking layer (e.g. Newberger and Allen, 2007; Uchiyama et al., 2010; Kumar et al., 2012). It should also be noted that in this research the effects of mean wave horizontal pressure gradient, vortex force (Andrews and McIntyre, 1978) and Stokes production terms were not included.

The momentum transfer from breaking waves to the ocean also reads as:

$$F^{\text{Out, wave}} = \frac{1}{c} S^{\text{ds, s}} \quad (10)$$

where $S^{\text{ds, s}} = S^{\text{ds, w}} + S^{\text{ds, br}}$ is the surface wave dissipation computed by the wave model (Jenkins, 1989; Melville and Rapp, 1985), and c is wave phase velocity. It is assumed that the surface wave momentum term has a decaying vertical distribution $\exp(-2k_w|z|)$.

The total stress from wind to ocean is defined as τ^{Wind} by:

$$\tau^{\text{Wind}} = \tau^{\text{in, Wave}} + \tau^{\text{in, Turb}} + \tau^{\text{in, Visc}} \quad (11)$$

Here, the $\tau^{\text{in, Wave}}$ is the stress from wind to waves, $\tau^{\text{in, Turb}}$ and $\tau^{\text{in, Visc}}$ are the ocean turbulence and viscous stresses. The momentum received by waves is transferred to the ocean via conservative and non-conservative forces (Uchiyama et al., 2010). To be consistent with the total momentum transfer from wind to ocean, we subtract the momentum gained by the waves from bulk wind drag (Jenkins, 1989; Tang et al., 2007; Bakhoday Paskyabi et al., 2012). Therefore, the final surface stress in the ocean model reads as:

$$\tau^{\text{in, Ocean}} = \tau^{\text{Wind}} - \tau^{\text{in, Wave}}, \quad (12)$$

and the upper boundary condition for the momentum equation is set to:

$$\rho v_{\text{turb}} \frac{\partial \mathbf{U}}{\partial z} = \tau^{\text{in, Ocean}}, \quad (13)$$

where $\mathbf{U} = (u, v)$ is the current velocity vector.

In the temperature equation, further terms are the specific heat capacity of water C_p , solar radiation I , and reference density ρ_0 . The molecular diffusivities for momentum, temperature and salinity are ν , ν' and ν'' , respectively. The eddy viscosities are given by:

$$\nu_{\text{turb}} = c_\mu k^{\frac{1}{2}} l, \quad \nu'_t = c'_\mu k^{\frac{1}{2}} l \quad (14)$$

and turbulence length scale, l , is defined as:

$$l = (c_\mu^0)^3 \frac{k^{3/2}}{\epsilon} \quad (15)$$

where $c_\mu^0 = 0.55$ and $\sigma_k = 1.96$. The parameters are $\sigma_\omega = 2$, $c_{\omega 1} = 0.56$, $c_{\omega 2} = 0.83$, and $c_{\omega 3} = 0.0$ for stable and $c_{\omega 3} = 1.0$ for unstable stratification (Wilcox, 1988). The turbulence dissipation rate, ϵ , is defined as:

$$\epsilon = (c_\mu^0)^4 k \omega \quad (16)$$

Umlauf et al. (2003) showed that for the two equation turbulence models discussed here, the turbulent kinetic energy, k , and length scale, l , in the wave-enhanced layer are computed by:

$$k = K(-z + h + z_0^s)^a, \quad l = L(-z + h + z_0^s) \quad (17)$$

where K , L and a are constant and z_0^s is surface roughness (Section 2.2.1).

Umlauf and Burchard (2003) demonstrated that the power laws in Eq. (17) are exact solutions of Eqs. (8) and (9), if a balance between diffusion and dissipation is assumed. With this assumption in mind, we can extend the modeling domain to the wave-enhanced layer (See Fig. 1). They further showed that a and L appearing in Eq. (17) are functions of the model parameters. The upper boundary condition

Table 1
The values proposed for surface roughness (z_0^s) and α^s in the literature.

Method	Proposed range	α^s	Specifications
Craig and Banner (1994)	$z_0^s = 0.1$ m	100–150	Using Mellor and Yamada (1982) turbulence model
Gemmrich and Farmer (1999)	$z_0^s = 0.2$ m	^a	Micro-structure measurements under large waves ($H_s = 3.5$ m)
Burchard (2001)	$0.2 < z_0^s/H_s < 1$	100	k - ϵ turbulence model with modified Schmidt number
Terray et al. (1999)	$z_0^s/H_s = 0.85$	100	Craig and Banner (1994) with modified length scale
Umlauf and Burchard (2003)	$z_0^s/H_s \approx 1$	100	k - ω via generic length scale model
Kantha and Clayson (2004)	$z_0^s/H_s = 1.6$	100	Assuming fully developed sea
Stips et al. (2005)	$z_0^s/H_s \ll 1$	100	Umlauf and Burchard (2003) for low wind condition in small lake
Feddersen and Williams (2007)	$z_0^s = 0.2$ m	250	They investigate white-capping type breaking in nearshore region in water depth of 3.5 [m].
Jones and Monismith (2008a)	$z_0^s/H_s = 1.3$	60	k - ω Shallow wind forced environment with tide

^a Instead of using the surface flux of the turbulence kinetic energy proportional to the cube of the surface friction velocity, they used $F_k^s = c_p u_*^2$ where $c_p = 0.8$ [m s^{-1}] is the effective phase speed of waves acquiring energy from the wind (Gemmrich et al., 1994).

for k , is defined by Eq. (3) for the TKE equation (Eq. (8)). Umlauf and Burchard (2003) also demonstrated that, based on the solutions in Eq. (17), using Eqs. (14)–(16), a flux boundary condition for the ω equation (Eq. (9)) can be derived. This boundary condition was also used in all our computations.

The surface flux of TKE, F_k^s , can be either parameterized based on surface wind friction velocity cubed (Craig and Banner, 1994; Terray et al., 1996) by $F_k^{s,\text{wind}} = \alpha^s u_*^3$, or directly obtained from an ocean wave model in terms of computed surface wave dissipation terms (Jenkins, 1989), by $F_k^{s,\text{wave}} = \beta^s S^{\text{ds},s}$; where u_*^s is the surface friction velocity and α^s and β^s are constant. From literature, $\alpha^s \approx (100\text{--}150)$ has been used in lakes and open oceans (Craig, 1996; Terray et al., 1996). Recently Feddersen et al. (2007) proposed $\alpha^s \approx 250$ for nearshore white-capping cases (see Table 1). $\beta^s \approx 1$ is proposed for deep water white-capping (Jenkins, 1989; Bakhoday Paskyabi et al., 2012) and $\beta^s \approx 0.01 \sim 0.15$ for depth-induced breaking (Govender et al., 2004; Huang et al., 2009; Feddersen, 2012a,b).

Surface roughness z_0^s (or, more precisely, Lz_0^s), is the length scale of turbulence injected at the top of the wave-enhanced layer. This parameter is an important factor which controls the vertical distribution of the TKE in the upper portion of the water column. However, measuring this parameter is difficult. In various numerical model studies this parameter was adjusted to produce closer results to available observations. Therefore, a relatively wide range of values for z_0^s are proposed. (See Table 1.) According to Stips et al. (2005), the magnitude of z_0^s also depends on the method of observation. For example $z_0^s > H_s$ was reported from a fixed tower measurement, but $z_0^s = 0.2$ [m] was calculated with a floating instrument for $H_s = 3.5$ [m] (Gemmrich and Farmer, 1999). In another example, Umlauf et al. (2003) showed that for $z_0^s = H_s$ results from a k - ω two-equation model compared best against WAVES (Terray et al., 1996) and SWADE (Drennan et al., 1996) datasets.

3. Methodology

3.1. Case study

The New River Inlet (NRI) is a tidal inlet on the Atlantic Coast in southeastern North Carolina, USA (NRI; blue rectangle in Fig. 2a). NRI is a relatively shallow tidal channel system. North Topsail Island and Onslow Beach are located at either side of the inlet entrance. A small amount of fresh water inflow at the upstream river, landward of the inlet entrance, does not create a significant salinity gradient in and around the inlet entrance. The inlet has a maximum tidal range of less than 2 [m] with tidal velocity maxima close to 2 [m s^{-1}] in the main channel. Incoming ocean waves with significant wave heights, H_s , greater than 1.5 [m], are expected during stormy conditions.

3.2. Data

NRI was the site of an intensive data collection effort in May–June 2012 as part of the Data Assimilation and Remote Sensing for Littoral

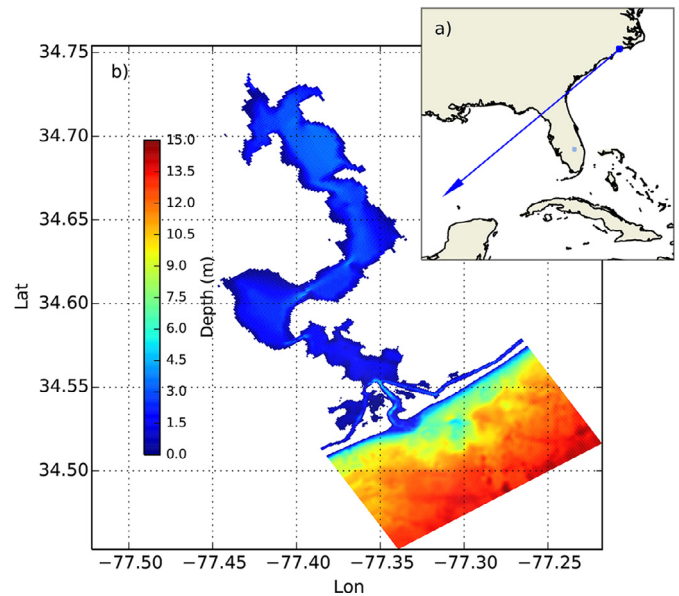


Fig. 2. Bathymetry of the New River inlet region. The blue rectangle shows the numerical model grid location. (a) The New River located on the Atlantic Ocean coast, and (b) model domain. (For interpretation of the references to color in this figure legend, the reader is referred to the web version of this article).

Applications (DARLA) project (Jessup et al., 2011). Observations included SWIFT buoys measurements, tower-based video, infrared, and radar, as well as airborne SAR and infrared observations. A simultaneous in-situ observational campaign for meteorology, current velocity and surface wave characteristics took place.

The five-minute averaged observations of TKE dissipation rate measured by SWIFT buoys were compared to model results. SWIFTs measured surface turbulence in a wave-following reference frame with an upward-looking, pulse-coherent Doppler sonar (2 MHz Aquadopp HR), which measured turbulence in a profile beneath the free surface (i.e., within ~ 0.5 m). The second-order structure function was calculated and used to infer the TKE dissipation rate following Kolmogorov's theoretical energy cascade. The SWIFT also measured wave spectra, winds, and mean surface currents (Zippel and Thomson, 2015; Thomson et al., 2014).

The second-order structure function was defined as $D(z, r) = \langle [u'(z) - u'(z+r)]^2 \rangle$, where u' is the turbulence fluctuation, z is the vertical location beneath the free surface, r is the along-beam lag distance between velocity measurements, and the angle bracket denotes the burst time average (5 min) (Thomson, 2012).

Six SWIFT buoys were operated daily for one month during the experiment at NRI. Sampling covered all tidal conditions and a range of wind-wave conditions.

Table 2
Settings for ROMS, SWAN and GOTM.

ROMS settings	
Version	3.4
Time step	2 [s]
Quadratic bottom drag coefficient	0.001
Tidal boundary condition	Oregon State University Tidal Inversion Software (OTPS; Egbert and Erofeeva, 2002)
Tidal constituents	k2, s2, m2, n2, k1, p1, o1, q1
Velocity boundary condition	Flather (1976)
Free surface boundary condition	Chapman (1985)
Grid spacing (Fig. 2b)	40–300 [m]
Grid size	$N_x = 170$ and $N_y = 400$
SWAN settings	
Version	40.91
Number of frequency bins	45 and 90
Number of direction bins	36
Mode	Stationary
Depth-induced breaking	Janssen and Battjes (2007)
Bottom friction	JONSWAP ($\gamma = 0.67$)
Quadruplets wave-wave interaction	Default coefficients
Boundary spectra	New River Inlet Buoy, CDIP Station 190
Wind forcing	Meteorological pile (Fig. 3)
Grid spacing (Fig. 2b)	40–300 [m]
Grid size	$N_x = 170$ and $N_y = 400$
GOTM settings	
Version	4.1
Number of vertical layers	300
Time step	2 [s]
Simulation period	2 [day]
z_{0min}^s	0.1 [m]

We chose SWIFT observations in which the wind speed is greater than $6 \text{ [m s}^{-1}\text{]}$ and the peak wave period is less than 6 [s] to minimize the effects of processes (e.g. swell waves), which are not included in this modeling approach (The method of prescribing surface flux of TKE was originally developed for locally generated wind waves (Craig, 1996; Terray et al., 1996; Greenan et al., 2001). We also chose water depths greater than 4 [m] to limit the contamination of surface wave dissipation by depth-limited wave breaking. Using these criteria, the majority of SWIFT locations were chosen from 07 and 18 of May 2012. Therefore 41 SWIFT locations, each of them with 10 measured turbulence dissipation rates, every 0.04 [m] from 0.02 [m] below the ocean surface were chosen. The locations of the selected SWIFT observations, and position of the pile were the meteorological data were collected by Applied Physics Laboratory of University of Washington, and the bottom-mounted pressure gauge and wave buoy were both operated by Woods Hole Oceanographic Institution (Wargula et al., 2014) are shown in Fig. 3.

3.3. The model system

The model system developed in this study consists of the Regional Ocean Modeling System (ROMS; Shchepetkin and McWilliams, 2003; 2005), the Simulating WAve nearshore (SWAN; Booij et al., 1999; 2004) and the General Ocean Turbulence Model (GOTM; Umlauf et al., 2005). The schematic flowchart of the data exchange among the models is presented in Fig. 4.

ROMS is a free-surface, terrain-following, primitive equations ocean model widely used by the scientific community for a diverse range of applications. We employed ROMS in a two-dimensional depth-averaged mode as the circulation component of the modeling system. ROMS provides the water level elevation and the depth-averaged ambient current to SWAN and the depth averaged ambient current to GOTM. SWAN is a phase-averaged spectral wave model that solves the action density equation and generates spectrally-integrated surface wave properties, significant wave height H_s , average wave length λ , mean relative wave period T , mean wave direction $\bar{\theta}$, and orbital velocity at the bottom, as well as the energy input

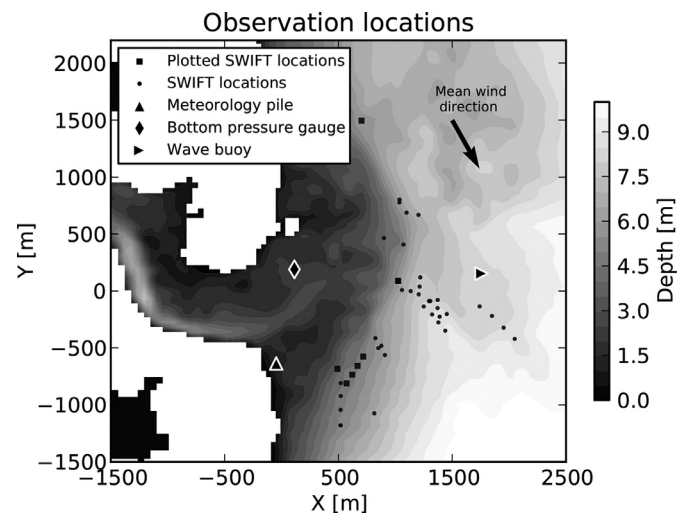


Fig. 3. Observation locations at New River Inlet. Circles and rectangles are SWIFT locations ($N = 41$). Diamond is the location of bottom mounted pressure gauge. The up- and right-triangles are the locations of the meteorological pile and wave buoys.

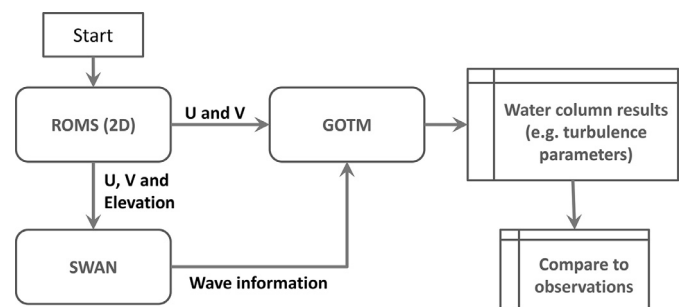


Fig. 4. The flowchart of coupling algorithm among models. ROMS (2D) and SWAN models run for the whole domain and time period. GOTM model was executed for each SWIFT observation location separately using information provided by ROMS(2D) and SWAN.

Table 3
SWAN wave model configurations.

	WavConf1 (SWAN defaults for GEN3 command)	WavConf2 (Mulligan et al., 2008)
Wind input (exponential)	Snyder and Elliott (1981)	Yan (1987)
White-capping	Komen et al. (1984)	Alves and Banner (2003)

from the wind to the wave field S^{in} , the dissipation rates due to bottom friction $S^{\text{ds,b}}$, surface wave breaking $S^{\text{ds,br}}$ and white capping $S^{\text{ds,w}}$ (Booij et al., 2004). These wave parameters are transferred to GOTM to calculate the wave forcing and the boundary conditions for the momentum and turbulence equations. GOTM is a one-dimensional water column model for the hydrodynamic processes related to vertical mixing in natural waters. The key characteristic of GOTM is its ability to calculate vertical turbulence fluxes using different turbulence closure models. In this study, we used a version of GOTM that includes implemented wave effects (Jenkins, 1989). More details about the implementation are given in Bakhoday Paskyabi et al. (2012). GOTM receives waves and depth-averaged velocity information, and calculates momentum turbulent fluxes and the TKE dissipation rate including surface waves and tidal effects. GOTM was executed (i.e., a 1DV ocean model) in a quasi-stationary mode (forced with time dependent boundary conditions) at each SWIFT measurement location. The model results were compared with the SWIFT observations (e.g. TKE dissipation rate profiles) at the same time of the passage of the drifter through each location. It should be noted that all model simulations start at least 2 days before the time of data-model comparison (minimum 2 days of spin up).

3.4. Model system setup

A variable rectangular grid, with higher spatial resolution at the inlet entrance and lower toward model boundaries, was employed (Fig. 2b). The computational grid, which is identical for both the wave and circulation models, encompasses the estuary, and extends offshore onto the continental shelf to water depths of 15 [m]. Specification of the common model settings for ROMS, SWAN and GOTM are given in Table 2.

The ROMS simulation was forced by 8 main tidal constituents derived using the Oregon State University Tidal Inversion Software (OTPS; Egbert and Erofeeva, 2002). The SWAN grid was forced at the open boundaries using boundary spectra from the New River Inlet Buoy (CDIP Station 190), which is located very close to south-east boundary of the model grid. For the offshore boundary, a spatially uniform spectra identical to CDIP buoy spectra was applied. For the sides of the domain, boundary spectra were generated using a one-dimensional SWAN model setup for each boundary forced by CDIP information at their offshore boundary points. The local Cartesian coordinate system (x, y) is introduced for presenting the results, where x is directed offshore and y is directed alongshore, respectively (Fig. 3).

As previously discussed, the surface roughness in the modeling studies was chosen based on the sensitivity analysis of the model in comparison to available observations. However, considering that the surface roughness reported in literature from floating measurement devices is generally smaller than for fixed measurement devices, and also based on some preliminary analyses of the SWIFT data for the estimation of turbulence length scale, we confined the range of the surface roughness length to $0.1-0.6H_s$. Based on sensitivity analysis reported in Appendix A, $z_0^s = 0.6H_s$ was the best choice regarding our available observational dataset.

Burchard (2001) proposed to apply the surface flux boundary condition at the base of the wave breaking layer with the thickness of z_0^s . However, based on our observational data set, locating the surface flux boundary condition in the middle of the wave breaking layer re-

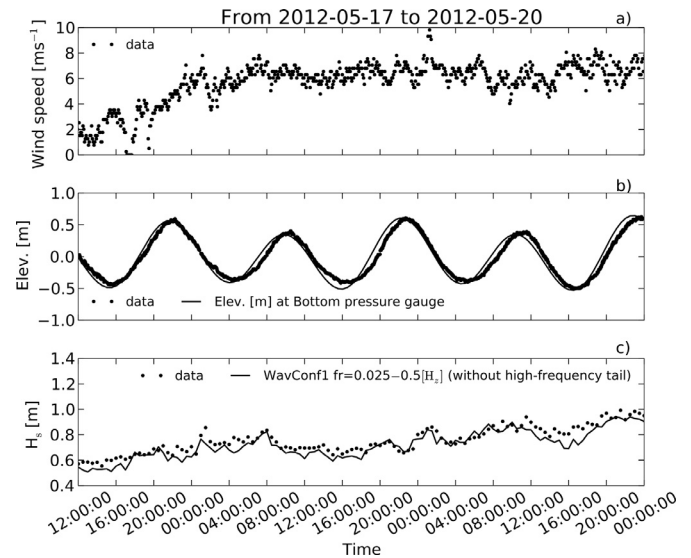


Fig. 5. Time series of the wind speed (a), water surface elevation (b), and significant wave height (in which both model and observation wave heights computed from model and measured spectra by integrating over the same frequency range $fr = 0.025-0.5$ Hz) (c). Black dots are the observations, and lines are the model results.

sulted in a better model and data comparison. Furthermore, our analysis of the vertical gradient of the TKE dissipation rate data showed that the nonlinear least square fit to the data below $0.5z_0^s$ distance from mean sea surface agrees closely with the Terray et al. (1996) transition layer slope of z'^{-2} (see Section 5.1).

3.5. Model system verification

The observations from in-situ measurement stations (Fig. 3) were used to validate ROMS and SWAN modeling results (Fig. 5). Wind speed observations from the meteorological pile, which were also used for forcing SWAN and GOTM, are shown in Fig. 5a. The data presented in this figure covers the period from May 17–20, 2012. The wind speed increased from calm conditions before May 18, 2012 to an average speed of $6 \text{ [m s}^{-1}]$, staying near constant (with some oscillations) until May 20, 2012. It should be noted that the wind data is available every 5 min, however, the wave model is executed every half hour. Therefore the half-hourly wind was used to calculate the wind-input source terms in SWAN.

The average wind direction is shown in Fig. 3 by a black vector, which is directed parallel to the shoreline and slightly towards offshore. This is consistent with our choice of SWIFT cases in locally generated wind wave conditions. The surface elevation produced by ROMS shows good agreement in comparison with observed surface elevation by the bottom mounted pressure gauge (Fig. 5b).

Two different configurations of SWAN were studied (Table 3). The common physical parameters for both configurations are given in Table 2. For the first configuration (WavConf1), the default parameterization for the third generation mode (GEN3) of SWAN, was chosen. In this setting, the method proposed by Snyder and Elliott (1981) for the exponential wind input source term and Komen et al. (1984) for the white-capping term were used. For the

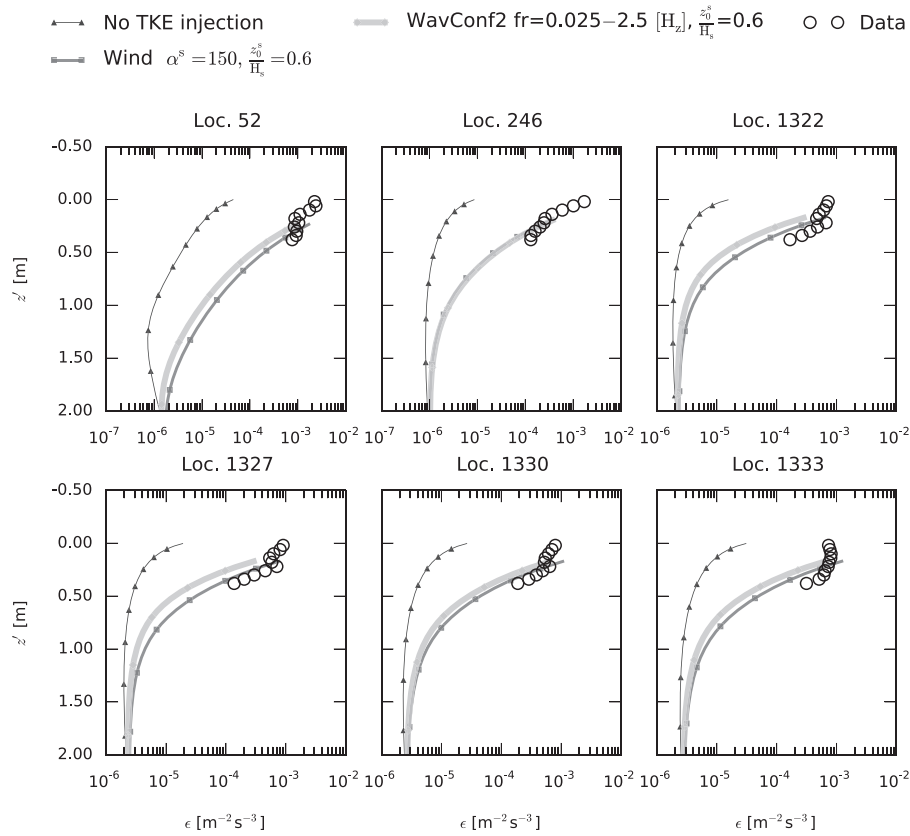


Fig. 6. Profiles of the turbulence dissipation rate (ϵ) at the top 2 [m] of the water column. The comparison made for three different TKE surface flux boundary condition results from a $k-\omega$ two equation turbulence closure model and the measured quantity from 5 min bursts averaged SWIFT observations. The observation locations are shown in Fig. 3 by 6 black rectangles.

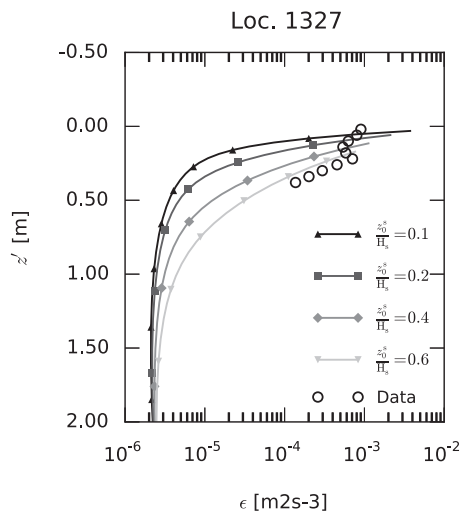


Fig. 7. Sensitivity of the turbulence dissipation rate (ϵ) profiles to the choice of z_0^s . The comparison made for four different surface roughness of $\frac{z_0^s}{H_s} = 0.1, 0.2, 0.3$ and 0.4 at location 1327. See description of Fig. 6.

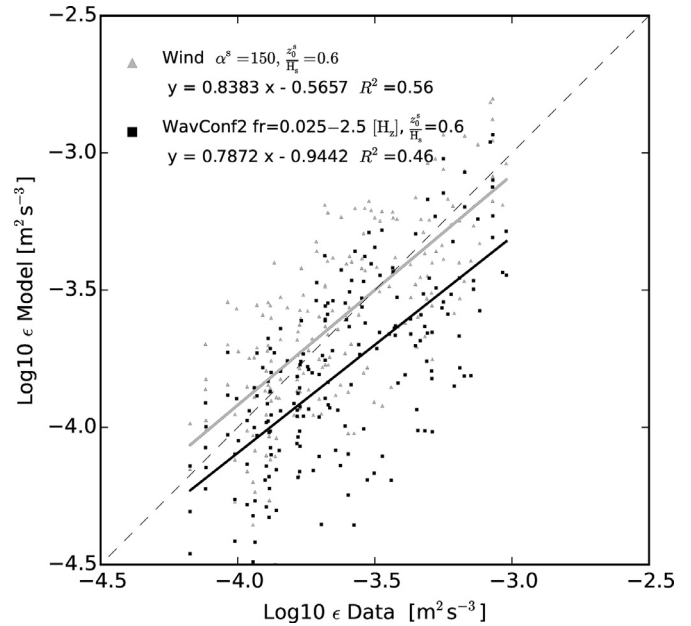


Fig. 8. Scatter plot of the measured and modeled turbulence dissipation rate (ϵ) using $k-\omega$ turbulence model. Model results of TKE injection by surface wind friction velocity cubed with $\alpha^s = 150$ and $\frac{z_0^s}{H_s} = 0.6$ are shown by blue triangles and TKE injection by wave model surface dissipation of Wavconf2 with $fr = 0.025-2.5$ [Hz], $\frac{z_0^s}{H_s} = 0.6$ are shown by green rectangles. (For interpretation of the references to color in this figure legend, the reader is referred to the web version of this article).

second configuration (WavConf2), the physical parameterization proposed by Mulligan et al. (2008) was applied. The method proposed by Yan (1987) was adopted for the exponential wind input term. This method reduces to Snyder and Elliott (1981) for low frequencies and to Plant (1982) for the high frequency part of the wave spectrum. The Alves and Banner (2003) method was selected for the white-capping term.

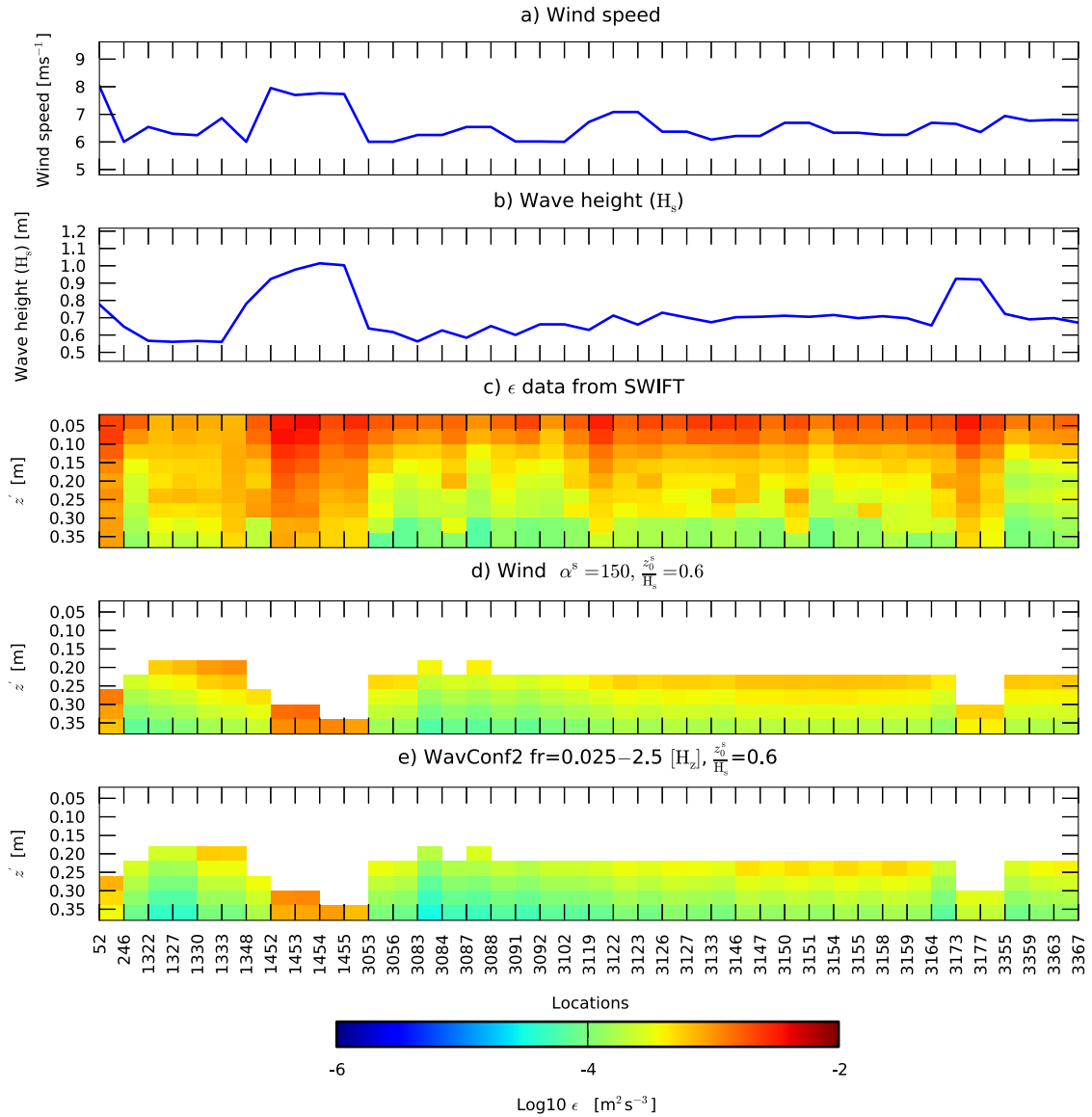


Fig. 9. Comparison of measured and modeled turbulence dissipation rate (ϵ) for all SWIFT locations. (a) Wind speed, (b) significant wave height, (c) SWIFT measurements, (d) modeled with TKE injection by surface wind friction velocity cubed with $\alpha^s = 150$ and $\frac{z_0^s}{H_s} = 0.6$ and (e) modeled with TKE injection by wave model surface dissipation of Wavconf2 with $fr = 0.025-2.5$ [Hz], $\frac{z_0^s}{H_s} = 0.6$.

Each SWAN configuration was executed for two different frequency ranges, 0.025–0.5 [Hz] (normal range) and 0.025–2.5 [Hz] (broad range). To resolve wave spectrum in the spectral dimension, 45 frequency bins for normal range and 90 bins for broad frequency ranges were chosen. The simulated significant wave height using WavConf2 and frequency range of 0.025–0.5 [Hz] are in agreement with the measurement (Fig. 5c).

4. Results

We carried out a comprehensive sensitivity analysis for different modeling parameters. The results of this analysis are presented in Appendix A. This analysis was done for the z_0^s in the range of 0.1–0.6 H_s , for the α^s parameter in the range of 100–400, for two different wave configuration of WavConf1 and WavConf2. Each wave configuration was tested for normal and broad frequency ranges. Hereafter, comparison of different methods for prescribing surface flux of TKE using a $k-\omega$ 1DV turbulence closure model for the best parameter set in each category based on the sensitivity analysis is presented. We compared three cases as: (1) No surface flux of en-

ergy (NoTKE), (2) TKE injection by surface wind friction velocity cubed with $\alpha^s = 150$ and $\frac{z_0^s}{H_s} = 0.6$ (WIND), and (3) TKE surface flux from wave model using WavConf2 and frequency range of 0.025–2.5 [Hz] and $\frac{z_0^s}{H_s} = 0.6$ (WAVE). It should be noted that the choice of $z_0^s = 0.6H_s$ is also consistent with previous studies (e.g. Terray et al., 1996; Soloviev and Lukas, 2003).

4.1. General comparison

The modeled turbulence dissipation rate, ϵ , of the top 2 [m] portion of the water column for 6 sample SWIFT locations, is presented in Fig. 6. The WIND, and WAVE models are in reasonable agreement with the measurements. The NoTKE case shows low skill and produced the TKE dissipation rates almost two orders of magnitude smaller than the measurements. All curves converge to the same value near 2 [m] below the mean sea surface, suggesting injection of turbulence could enhance the TKE dissipation rate to depths almost 3 times that of the significant wave height.

An example of comparison of the effects of different z_0^s on the vertical profile of turbulence dissipation rate is presented in Fig. 7.

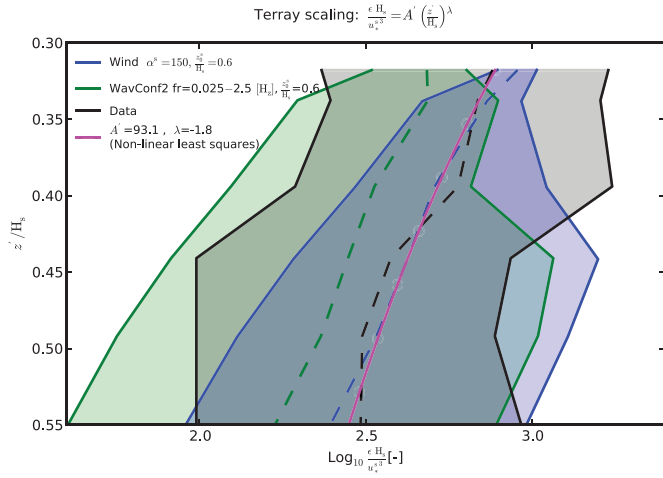


Fig. 10. Terray-scaled $\epsilon H_s / u_w^3$ against z' / H_s for white-capping observation using 216 data points at 41 locations out of a total of 410 observations (see Fig. 3). The model results for TKE injection by surface wind friction velocity cubed with $\alpha^s = 150$ and $\frac{z_0^s}{H_s} = 0.6$ are shown by the blue area, TKE injection by wave model surface dissipation of Wavconf2 with $fr = 0.025-2.5$ [Hz], $\frac{z_0^s}{H_s} = 0.2$ are shown by the green area and the data represents by the gray area. All dash lines are the horizontal average of their corresponding values in the same vertical level. The magenta line is the non-linear least squares fit to the data. (For interpretation of the references to color in this figure legend, the reader is referred to the web version of this article).

Smaller surface roughness results in poor agreement between model and data. Also, a model surface offset of half surface roughness in the case of $z_0^s = 0.6H_s$ seems to be appropriate, as the model starts at the same level and with the same vertical gradient as the data.

The results obtained from WIND and WAVE cases together with their corresponding data are presented in the form of a scatter plot in Fig. 8. There is general agreement between measurements and model results for both WIND and WAVE cases. Index of agreement for WIND, WAVE and NoTKE cases are 0.84, 0.78 and 0.42, which indicates slightly better performance of the WIND case. The r-squared values of WIND and WAVE cases are 0.56 and 0.46, which also show better agreement of WIND in comparison with the observations (see Appendix A).

4.2. Vertical variation of the turbulence dissipation rate (ϵ)

Profiles of the turbulence dissipation rate for all observation locations are presented in Fig. 9. A positive correlation is shown between wind speed observations (Fig. 9a), modeled wave height (Fig. 9b) and TKE dissipation rate data. This is expected because the majority of selected locations are situated in a locally generated wind wave sea state, and white-capping breaking is an active sink of energy for surface waves. It should be noted that the masked areas in the model results correspond to the regions which are not covered by the model because these points are above the position of the TKE surface flux boundary condition. Therefore, for the locations with greater wave heights, less data points for comparison with the modeling results are available.

Some of the events in this figure are distinctive. For instance, profile 52, which was observed at 18:47 May 1, 2012 [UTC], shows coexistence of a relatively high wind speed and wave height with a high turbulence dissipation rate in the data and both WIND and WAVE model results (Fig. 9d and e). There is another storm event at profiles 1452–1455, which occurred around 18:00 May 7, 2012. A strong correlation between wind speed and wave height again show that locally generated wind waves are dominant. A very high dissipation rate in the data represents a large amount of TKE injected by white-capping dissipation. The SWIFT data and model results are in agree-

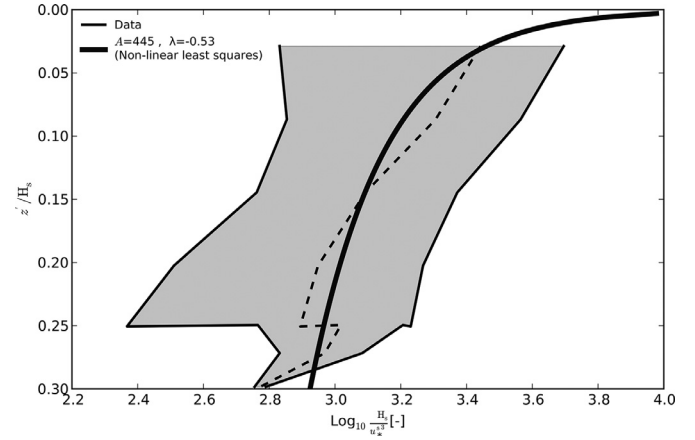


Fig. 11. Terray-scaled $\epsilon H_s / u_w^3$ against z' / H_s for white-capping observation using 194 data points at 41 locations out of total number of 410 points (see Fig. 3). The gray area represents the measurements. The dashed line is the average of the data in the same vertical level. The magenta line is the non-linear least squares fit to the data.

ment and a relatively high turbulence dissipation rate is still evident up to ~ 0.4 [m] below the water surface. In general both WIND and WAVE model results are in agreement with the SWIFT measurement.

5. Discussion

5.1. Terray scaling

Terray et al. (1996) proposed a three layer system for the near-surface turbulence dissipation rate in the presence of locally generated wind waves. They defined the top layer as the breaking zone with direct injection of turbulence from wave breaking with a constant TKE dissipation rate, ϵ_b . They also suggest that the thickness of this layer, z'_b , could be estimated by $\frac{z'_b}{H_s} = 0.6$. Beneath this layer, there is another layer in which the TKE dissipation rate is a function of energy input F_k^s , wave height H_s and z' , as below:

$$\frac{\epsilon H_s}{F_k^s} = \beta_T \left(\frac{z'}{H_s} \right)^\lambda \quad (18)$$

in which $\beta_T = 0.3$ and $\lambda = -2$. This layer will also be transitioned to a deeper layer at depth of z'_t where the wall layer scaling is applicable,

$$\epsilon = \frac{u_*^3}{\kappa z'}. \text{ Here } \kappa = 0.41 \text{ is the von Karman constant.}$$

However, Gemmrich and Farmer (2004) showed that their observations with a floating device agree with Stewart and Grant (1962) who suggested that the dissipation at a fixed distance beneath the wave crest and trough are different, which is not supportive of the existence of the constant dissipation layer proposed by Terray et al. (1996). On the other hand, Feddersen (2012a) showed the applicability of Eq. (18) with $\lambda \simeq -2$ in the transitional region, which is almost one significant wave height below the water surface ($\frac{z'_b}{H_s} \simeq 1$).

In this study, employment of the 5 min averaged observational TKE dissipation rate profiles seems to be an appropriate choice for comparison with modeling results, since both wave and hydrodynamic models employ wave averaged properties. In addition, SWIFT observations contain most of the active wave breaking areas at crests and troughs, which are happening around the mean sea surface. In other words, one can assume that a substantial part of the measured data is taken within the half of z_0^s from the mean sea surface which is not taken into account by the model (the blank regions in Fig. 9d and e).

The choice of the location of surface flux of TKE, to be situated at half of the surface roughness length at $z' \simeq 0.3H_s$ was also

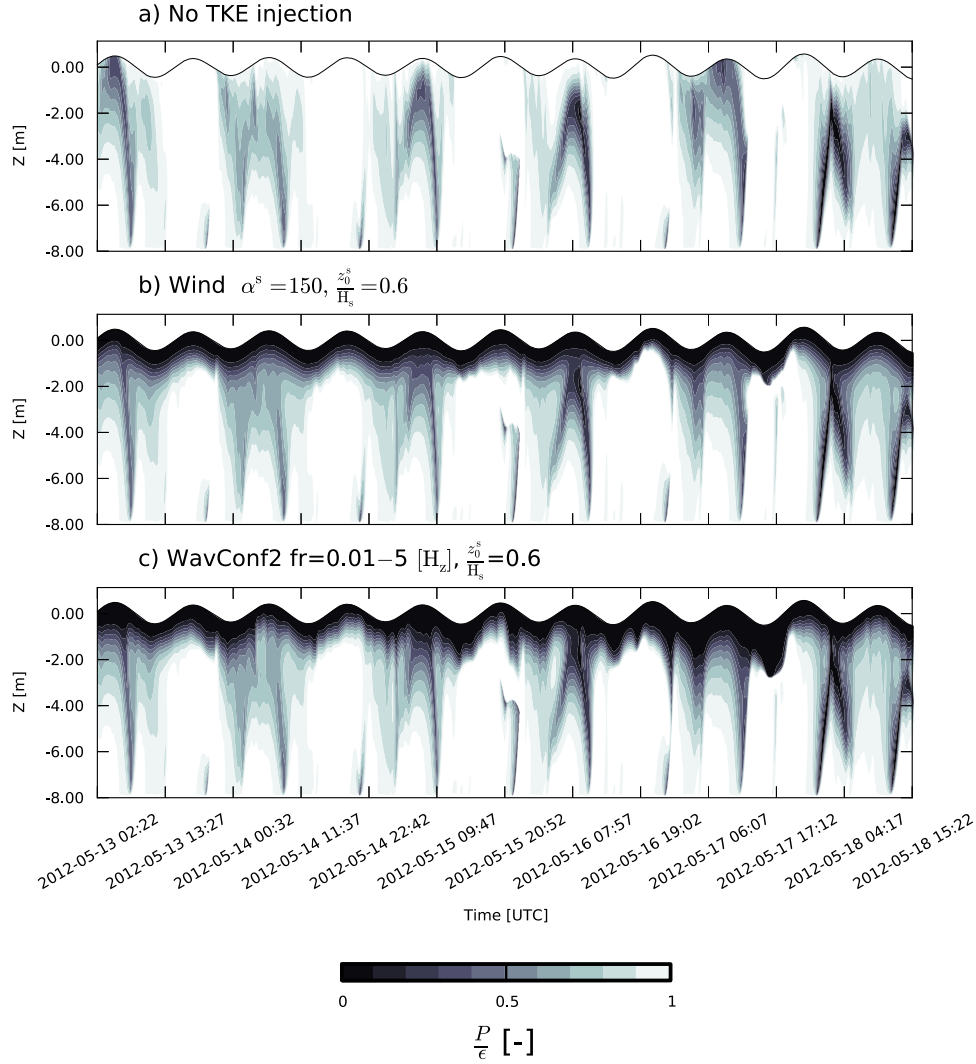


Fig. 12. Ratio of shear production of TKE (P) to turbulence dissipation rate (ϵ) at location 3123.

motivated by our analysis over available data which shows a change in the slope of the turbulence dissipation rate profiles around this distance from ocean surface (e.g. see Fig. 7). We also examined the proposed equation by Terray et al. (1996) as:

$$\frac{\epsilon H_s}{u_*^3} = A' \left(\frac{z'}{H_s} \right)^\lambda \quad (19)$$

assuming $F_k^s = \alpha^s u_*^3$ then $A' = \beta_T \alpha^s$.

Non-dimensionalized model-data comparisons following the method proposed by Terray et al. (1996) are given in Fig. 10. The magenta colored line represents the non-linear least square fit over the data in this portion of the water column. The best fit resulted in $\lambda = -1.8$, which is also comparable with $\lambda = -2$ proposed by Terray et al. (1996). Assuming $\alpha^s = 150$, the $\beta_T = 0.62$ could also be calculated. The model results forced by TKE surface flux calculated directly from wind match with the non-linear least square fit.

We also applied the non-linear least square method to the SWIFT data close to the water surface above $z' \simeq 0.3H_s$ (Fig. 11). For this region, $\lambda = -0.53$ and $A' = 445$ were calculated. This is contrary to the top layer definition of Terray et al. (1999), with a constant turbulence dissipation rate. Given the negative gradient in TKE dissipation rate, it seems that the diffusion of the injected energy starts right below the wave averaged water surface.

5.2. Wave enhanced region

We employed the P/ϵ ratio to investigate the region influenced by wave breaking inside the water column. Here P refers to TKE production due to shear generated by bed or wind shear stresses (Term P in Eq. (8)). $P/\epsilon \simeq 0$ is associated with the regions with no shear production, e.g. near the surface, where turbulence is due to the downward diffusion of TKE injected by wave-breaking at the surface (Umhlauf and Burchard, 2003). Time evolution of this parameter at profile 3123 from the 13th until the 18th of May 2012 [UTC] is shown in Fig. 12. As it is apparent from Fig. 12a, when the surface flux of TKE due to surface wave dissipation is not included, there are frequent times where shear production and dissipation rates are in perfect balance throughout the whole water column. However, wave induced surface flux of TKE adds a new region of $P/\epsilon = 0$ starting from the surface towards the bottom, which we define as the wave enhanced region. Based on the modeling results, the assumption that the depth of the wave-enhanced layer is almost 3 times of the significant wave height (for this SWIFT location $H_s \simeq 0.8$ [m]) can be used as a crude approximation (Fig. 12b and c).

5.3. Effects of wave parameterization

Comparison of the wind input, surface dissipation and significant wave height for different wave configurations and frequency ranges

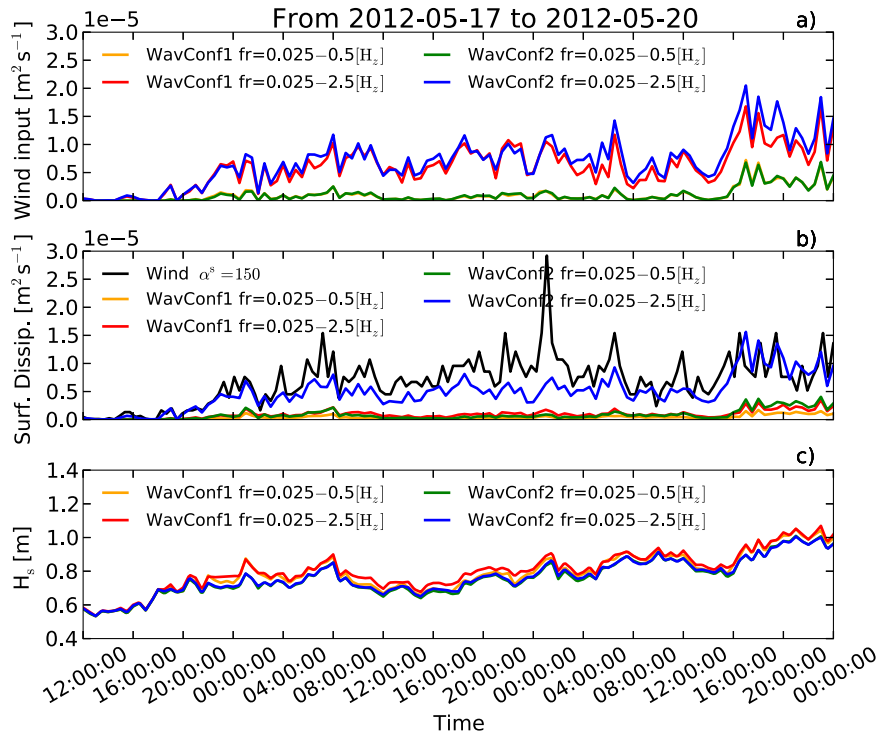


Fig. 13. Time series of wave model wind input source term (a), wave model surface dissipation sink term (b) and significant wave height (c). The black line in the bottom panel is calculated for equivalent surface dissipation based on surface flux of TKE from surface shear velocity cubed ($S_k^{ds} = F_k^s = \alpha^s u_*^3$ for $\alpha^s = 150$).

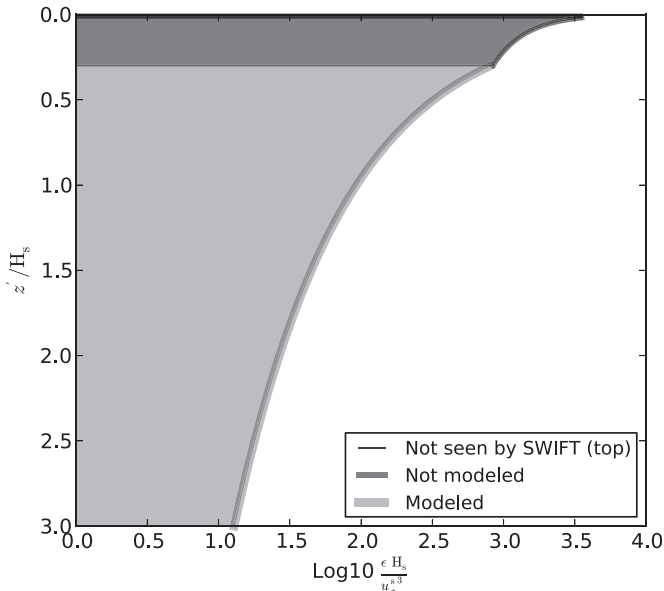


Fig. 14. Three regions of turbulence dissipation rate based on SWIFT observations and model results. Top layer where $z' < 0.02$ is the region which was not observed by SWIFT (ϵ^{top}) is shown by black. The beneath layer $0.02 < z' < 0.3H_s$ is the portion of water column which was not modeled ($\epsilon^{not_modeled}$) is shown by dark gray. The third layer which is covered by model and continued further down to $z' \approx 3H_s$ ($\epsilon^{modeled}$) is shown by light gray.

(see Table 3) are discussed hereafter. The normal frequency range for both wave model configurations produced similar outcomes for wind input source and surface dissipation sink terms (Fig. 13a and b). For the broad frequency range, the wind input source term increased similarly for both configurations. However, this was not the case for the surface dissipation. It seems that the white-capping dissipation term based on Komen et al. (1984) does not account for the wave dissi-

ipation in the high frequency tail of the spectrum and produces almost the same result as the normal frequency range. In contrast, surface dissipation computed using the Alves and Banner (2003) method (Wavconf2) shows an increase with the same order of magnitude as the increase in the wind input source term. This inconsistency is reflected in the significant wave height magnitude where the wave heights resulting from Wavconf2 for both frequency ranges are the same. However, the wave height resulting from Wavconf1 increased when we switched from normal to broad frequency range (Fig. 13c).

The white-capping formulations of Komen et al. (1984) and Alves and Banner (2003) methods are based on different physical assumptions. The first method computes the white-capping dissipation from wavenumber and some of the spectrally integrated parameters, such as the average wave steepness; however, the latter considers the wavenumber-dependent properties of the spectrum. For instance, employing the Komen et al. (1984) method in situations when energy in the low-frequency part of the wave spectrum is present, could lead to a significant effect on the averaged spectrum properties and results in an underestimation of the white-capping dissipation and overestimation of the wave height. Mulligan et al. (2008) showed that the difference between these white-capping dissipation methods could be significant (up to 3 times) for wind ranges from 5 to 17 [$m s^{-1}$] and the modified Alves and Banner (2003) model proposed by van der Westhuysen et al. (2007) generally showed a better agreement with their wave energy dissipation observations.

To be able to compare surface flux of energy received directly from the wave model to the one generated based on surface friction velocity, an equivalent surface dissipation using $S_k^{ds} = F_k^s = \alpha^s u_*^3$ for $\alpha^s = 150$ was calculated (black line in Fig. 13b). Interestingly, the amount of surface dissipation estimated from surface friction velocity (black line in Fig. 13b) and the one reported by the wave model using Wavconf2 (blue line in Fig. 13b) are in agreement. This was implicitly shown by similar turbulence dissipation rates resulting from these methods (see Figs. 8–10).

The workaround here might be to operate a wave model as usual with a normal frequency range, implement an analytical function to

estimate white-capping dissipation at the high frequency tail of the spectrum, and add it to the dissipation calculated by the model at the post-processing step. Later this final value of surface dissipation has to feed into the turbulence model as the surface boundary condition of TKE.

To quantify this finding, we investigated the amount of energy seen by SWIFT but not resolved within our model simulations. Using non-linear least square fit coefficient (see Figs. 10 and 11), we investigated the energy dissipation in three distinct vertical layers (Fig. 14), where $z' < 0.02$ is the uppermost region not observed by SWIFT (ϵ^{top}), and assuming a constant dissipation rate. The layer $0.02 < z' < 0.3H_s$ is the portion of the water column which was not modeled ($\epsilon^{\text{not_modeled}}$). We continued the third layer to $z' \approx 3H_s$ to account for all turbulence dissipation rates, penetrated all the way to the depth of the wave-enhanced layer ($\epsilon^{\text{modeled}}$). We calculated the ratio of the amount of the turbulence dissipation rate below and above the model origin from the plotted curves as:

$$\frac{\int \epsilon^{\text{top}} + \int \epsilon^{\text{not_modeled}}}{\int \epsilon^{\text{modeled}}} \simeq 1.8 \quad (20)$$

We assume that a substantial part of the measured turbulence dissipation rate is induced by the injection of energy from dissipated waves, which also could be supported by the strong correlation between high wind, high waves and measured turbulence dissipation rates shown in Fig. 9. We argue that the flux of energy coming out of the wave field as computed by the wave model is not even close to being sufficient. Although by changing the physical parameterization and using a broad frequency range, we were able to increase the predicted surface dissipation, but it still appears to be insufficient. Apparently, spectral wave models so far were parameterized and calibrated in a way to conserve the total energy budget and produce correct wave heights for a normal frequency range. In a global sense this means that, the flux of energy going into the wave field ($F_k^{\text{s, wave, in}} = S^{\text{in}}$) and the flux of energy coming out of wave field ($F_k^{\text{s, wave, out}} = S^{\text{ds, s}}$) are not necessarily similar to what happens in nature in terms of energy exchange between atmosphere, wave and ocean.

6. Summary and conclusion

The primary result of this study was to validate the consistency and applicability of state-of-the-art wave–ocean coupled modeling systems in terms of energy exchange between surface waves and the ocean water column. We set up a modeling system similar to the common fully coupled three-dimensional wave–ocean frameworks. The system consists of the SWAN wave model, the ROMS ocean model in two-dimensional depth integrated mode and GOTM, which is a one-dimensional vertical water column model that includes state-of-the-art two-equation turbulence closure models. Since we computed the water column properties only at observation locations, the system was not computationally demanding and we could test many different configurations and turbulence parameterization. Therefore we were able to employ a very high resolution k – ω two-equation turbulence closure model and perform a comprehensive sensitivity analysis. Based on the sensitivity analysis, the optimum values for key parameters of a turbulence model, e.g. surface roughness length and white-capping parameterization and wave frequency range, were determined (see Appendix A). From this analysis, the optimum roughness length of $\frac{z_0^s}{H_s} = 0.6$ was proposed. Based on our unique data set with very high resolution turbulence dissipation rate profiles close to the ocean surface, we were able to identify the optimal level for the application of the surface flux boundary condition in our one-dimensional vertical model, which is at half the surface mixing length below the mean sea surface. This resulted in a good agreement between the modeled turbulence dissipation rate and

measurements. Furthermore, in the modeled region, the non-dimensional Terray scaling with power of $\lambda = -1.8$ (instead of $\lambda = -2$), is applicable. The portion of the water column above the modeled region up to the closest SWIFT measurement to the averaged surface is more uniform in comparison to the second layer, however, it does not have constant dissipation rate as suggested by Terray et al. (1996).

The wave-enhanced layer thickness, based on a suggestion of Burchard (2001), is almost three times the significant wave height. White-capping, which takes place in the high frequency tail of the wave spectrum, is crucial for generating an amount of wave surface dissipation that can explain the observed turbulence dissipation rate. However, in spite of the agreement between the modeled TKE dissipation rate and SWIFT measurements inside the wave enhanced layer, we argue that the wave model still produced less wave dissipation in comparison to the measurements, referring to the amount of energy seen by SWIFT which is not included in modeling domain.

To be able to correctly parameterize and include the energy and momentum input from the surface wave field to the ocean water column, further investigation on wave dissipation sink terms (implemented in wave models) is needed. Having access to high temporal and spatial resolution turbulence dissipation rate measurements, from the ocean surface down to at least 2–3 times of the significant wave height, is necessary to minimize the uncertainties and help in developing accurate parameterization of turbulence models.

Acknowledgments

This research was supported by the Office of Naval Research Grant N00014-10-1-0932. L. Umlauf is grateful for the support by the German Ministry for Education and Research (BMBF) via Grant 03D0666A (project SECOS). We wish to thank the USACE-FRF staff, for providing bathymetric data. The authors would like to acknowledge Prof. Rob Holman and Prof. Falk Feddersen for many constructive discussions. We also thank Prof. Alastair Jenkins for providing GOTM model with implemented wave forcing. We would like to thank Prof. Steve Elgar and Prof. Britt Raubenheimer for providing in-situ measurements, Mr. Joe Talbert and Mr. Alex Deklerk for operation and maintenance of the SWIFT buoys and Mrs. Jean S. Donovan for proof-reading of the manuscript.

Appendix A. Sensitivity analysis of the modeling parameters

In order to quantitatively compare results from different cases, the index of agreement (IA) as defined in Willmott (1982), bias and root mean square error (RMSE) were calculated as:

$$\begin{aligned} IA &= 1 - \frac{\sum (X_{\text{model}} - X_{\text{data}})^2}{\sum (|X_{\text{model}} - \bar{X}_{\text{data}}| + |X_{\text{data}} - \bar{X}_{\text{data}}|)^2}, \\ \text{bias} &= \frac{1}{M} \left(\sum X_{\text{model}} - \sum X_{\text{data}} \right), \\ \text{RMSE} &= \frac{1}{M} \sqrt{\sum (X_{\text{model}} - X_{\text{data}})^2}, \end{aligned} \quad (1)$$

where X_{data} are observation, \bar{X}_{data} is observation mean, X_{model} are model results and M is the number of available observations.

In the first set of experiments, sensitivity of the modeled turbulence dissipation rate to the surface roughness z_0^s and α^s were investigated. As shown in Fig. A.1, the model run with $z_0^s/H_s = 0.6$ and $\alpha^s = 150$ produced less erroneous results. The model result with this setting produced almost zero bias, while it shows minimum error of $\text{RMSE} = 2e-4 \text{ [m}^2 \text{ s}^{-3}\text{]}$ and maximum index of agreement as $IA = 0.85$. Additionally, a separate set of cases were examined to study effects of frequency range and wave parameterization within the wave model. The results of this experiment are presented in Fig. A.2. From

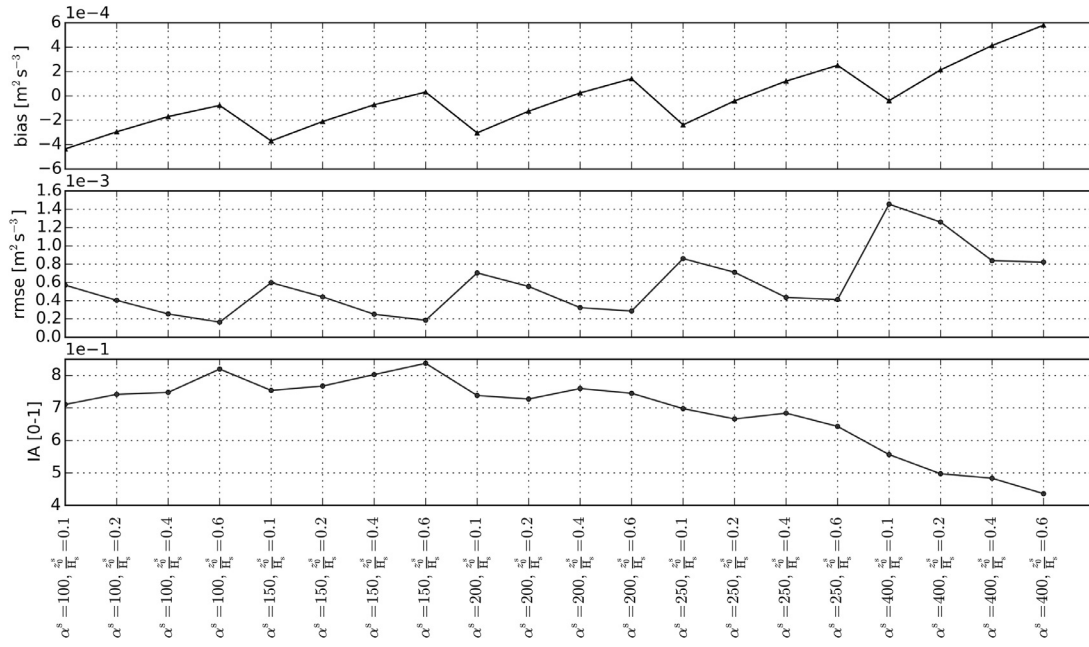


Fig. A.1. Sensitivity analysis experiment for investigating the effects of the surface roughness (z_0^s) and α^s on turbulence dissipation rate modeling results.

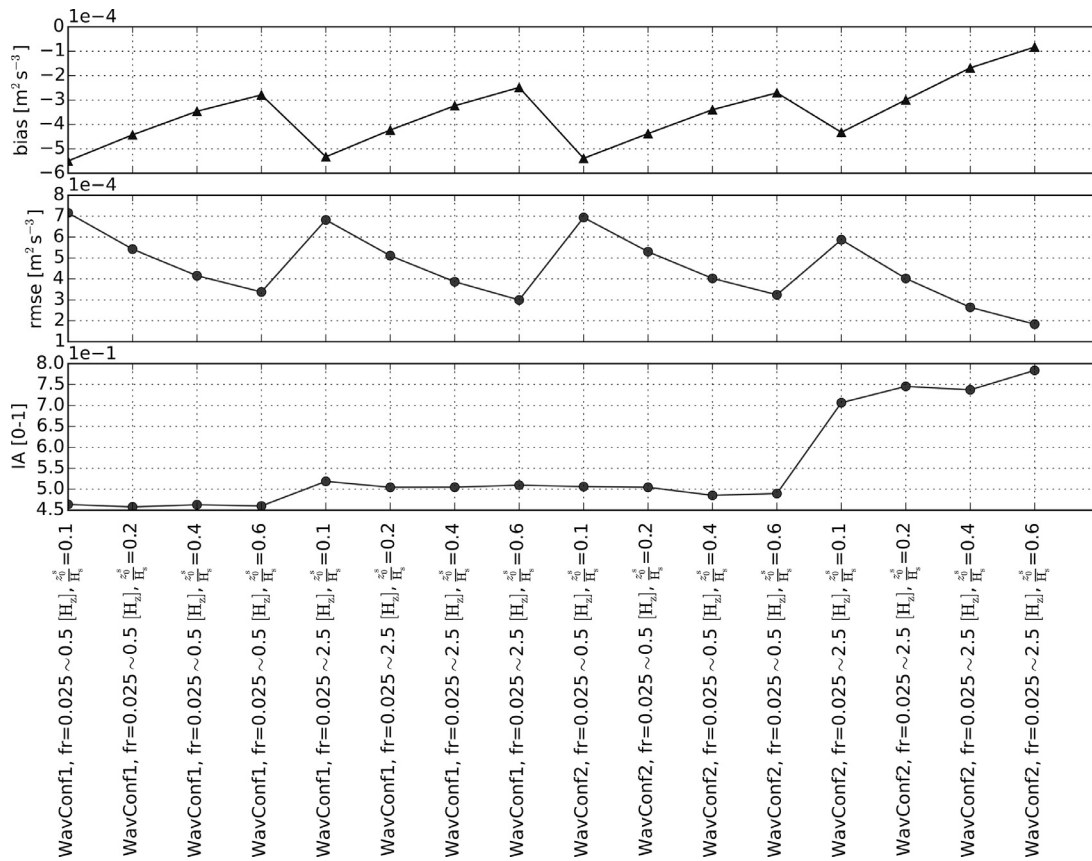


Fig. A.2. Sensitivity analysis experiment for investigating the effects of the wave model parameterization and spectral frequency range on turbulence dissipation rate modeling results.

this experiment, it seems the model results using WavConf2 and frequency range of 0.025–2.5 [Hz] and $\frac{z_0^2}{H_c} = 0.6$ produces less erroneous results. The model result with this setting produced almost zero bias, while it shows minimum error of RMSE = $2e-4$ [$m^2 s^{-3}$] and maximum index of agreement as IA = 0.78. It is worth mentioning that in almost all cases, the calculated bias is negative. This means that the model calculated dissipation rate is generally smaller than measured ones. There is also a dramatic improvement in increasing the frequency range from normal to broader range in case of WavConf2.

References

- Aiki, H., Greatbatch, R.J., 2014. A new expression for the form stress term in the vertically Lagrangian mean framework for the effect of surface waves on the upper ocean circulation. *J. Phys. Oceanogr.* 44 (1), 3–23.
- Alves, J.H.G., Banner, M.L., 2003. Performance of a saturation-based dissipation-rate source term in modeling the fetch-limited evolution of wind waves. *J. Phys. Oceanogr.* 33 (6), 1274–1298.
- Andrews, D., McIntyre, M., 1978. An exact theory of nonlinear waves on a lagrangian-mean flow. *J. Fluid Mech.* 89 (04), 609–646.
- Arduhin, F., Rasche, N., Belibassakis, K., 2008. Explicit wave-averaged primitive equations using a generalized Lagrangian mean. *Ocean Modell.* 20 (1), 35–60.
- Bakhoday Paskyabi, M., Fer, I., Jenkins, A.D., 2012. Surface gravity wave effects on the upper ocean boundary layer: modification of a one-dimensional vertical mixing model. *Cont. Shelf Res.* 38, 63–78.
- Booij, N., Haagsma, L., Holthuijsen, L., Kieftenburg, A., Ris, R., Van Der Westhuysen, A., Zijlema, M., 2004. SWAN cycle III version 40.41 user manual. Technical Report, Delft University of Technology.
- Booij, N., Ris, R., Holthuijsen, L., 1999. A third-generation wave model for coastal regions. I: model description and validation. *J. Geophys. Res.* 104 (C4), 7649–7666.
- Burchard, H., 2001. Simulating the wave-enhanced layer under breaking surface waves with two-equation turbulence models. *J. Phys. Oceanogr.* 31, 3133–3145.
- Carniel, S., Warner, J.C., Chiggiato, J., Scavo, M., 2009. Investigating the impact of surface wave breaking on modeling the trajectories of drifters in the northern Adriatic Sea during a wind-storm event. *Ocean Modell.* 30 (2–3), 225–239.
- Chapman, D.C., 1985. Numerical treatment of cross-shelf open boundaries in a barotropic coastal ocean model. *J. Phys. Oceanogr.* 15 (8), 1060–1075.
- Craig, P., 1996. Velocity profiles and surface roughness under breaking waves. *J. Geophys. Res.* 101 (C1), 1265–1277.
- Craig, P., Banner, M., 1994. Modeling wave-enhanced turbulence in the ocean surface layer. *J. Phys. Oceanogr.* 24 (12), 2546–2559.
- Drennan, W.M., Donelan, A.A., Terray, E.A., Katsaros, K.B., 1996. Oceanic turbulence dissipation rate measurements in SWADE. *J. Phys. Oceanogr.* 26, 808–815.
- Egbert, G.D., Erofeeva, S.Y., 2002. Efficient inverse modeling of barotropic ocean tides. *J. Atmos. Ocean. Technol.* 19 (2), 183–204.
- Fedderson, F., 2012a. Observations of the surf-zone turbulent dissipation rate. *J. Phys. Oceanogr.* 42 (3), 386–399.
- Fedderson, F., 2012b. Scaling surf zone turbulence. *Geophys. Res. Lett.* 39 (18), 1–5.
- Fedderson, F., Trowbridge, J.H., 2005. The effect of wave breaking on surf-zone turbulence and alongshore currents: a modeling study*. *J. Phys. Oceanogr.* 35 (11), 2187–2203.
- Fedderson, F., Trowbridge, J.H., Williams III, A., 2007. Vertical structure of dissipation in the nearshore. *J. Phys. Oceanogr.* 37 (7), 1764–1777.
- Fedderson, F., Williams III, A., 2007. Direct estimation of the Reynolds stress vertical structure in the nearshore. *J. Atmos. Ocean. Technol.* 24 (1), 102–116.
- Flather, R., 1976. A tidal model of the North–West European continental shelf. *Mem. Soc. R. Sci. Liege* 10 (6), 141–164.
- Gemmrich, J., Mudge, T., Polonichko, V., 1994. On the energy input from wind to surface waves. *J. Phys. Oceanogr.* 24 (11), 2413–2417.
- Gemmrich, J.R., Farmer, D.M., 1999. Near-surface turbulence and thermal structure in a wind-driven sea. *J. Phys. Oceanogr.* 29, 480–499.
- Gemmrich, J.R., Farmer, D.M., 2004. Near-surface turbulence in the presence of breaking waves. *J. Phys. Oceanogr.* 34 (5), 1067–1086.
- Gerbi, G.P., Chant, R.J., Wilkin, J.L., 2013. Breaking surface wave effects on river plume dynamics during upwelling-favorable winds. *J. Phys. Oceanogr.* 43 (9), 1959–1980.
- Govender, K., Mocke, G., Alport, M., 2004. Dissipation of isotropic turbulence and length-scale measurements through the wave roller in laboratory spilling waves. *J. Geophys. Res.* 109 (C8), 1–8.
- Grasso, F., Castelle, B., Ruessink, B., 2012. Turbulence dissipation under breaking waves and bores in a natural surf zone. *Cont. Shelf Res.* 43, 133–141.
- Greenan, B.J., Oakey, N.S., Dobson, F.W., 2001. Estimates of dissipation in the ocean mixed layer using a quasi-horizontal microstructure profiler. *J. Phys. Oceanogr.* 31 (4), 992–1004.
- Huang, Z.-C., Hsiao, S.-C., Hwang, H.-H., Chang, K.-A., 2009. Turbulence and energy dissipations of surf-zone spilling breakers. *Coast. Eng.* 56 (7), 733–746.
- Janssen, T., Battjes, J., 2007. A note on wave energy dissipation over steep beaches. *Coast. Eng.* 54 (9), 711–716.
- Jenkins, A., 1987. Wind and wave induced currents in a rotating sea with depth-varying eddy viscosity. *J. Phys. Oceanogr.* 17 (7), 938–951.
- Jenkins, A., 1989. The use of a wave prediction model for driving a near-surface current model. *Ocean Dyn.* 42 (3), 133–149.
- Jessup, A.T., Chickadel, C., Farquharson, G., Thomson, J., Holman, R.A., Haller, M., Kurovov, A., Özkan-Haller, T., Elgar, S., Raubenheimer, B., 2011. DARLA: data assimilation and remote sensing for littoral applications. Technical Report, DTIC Document, Office of Naval Research.
- Jones, N., Monismith, S., 2008a. The influence of whitecapping waves on the vertical structure of turbulence in a shallow estuarine embayment. *J. Phys. Oceanogr.* 38, 1563–1580.
- Jones, N., Monismith, S., 2008b. Modeling the influence of wave-enhanced turbulence in a shallow tide- and wind-driven water column. *J. Geophys. Res.* 113 (C3), C03009.
- Kantha, L., Clayson, A.C., 2004. On the effect of surface gravity waves on mixing in the oceanic mixed layer. *Ocean Modell.* 6 (2), 101–124.
- Kitaigorodskii, S.A., Donelan, M.A., Lumley, J.L., Terray, E.A., 1983. Wave turbulence interactions in the upper ocean. Part II: Statistical characteristics of wave and turbulent components of the random velocity field in the marine surface layer. *J. Phys. Oceanogr.* 13, 1988–1999.
- Komen, G., Cavaleri, L., Donelan, M., Hasselmann, K., Hasselmann, S., Janssen, P., 1994. Dynamics and Modelling of Ocean Waves. Cambridge University Press.
- Komen, G., Hasselmann, K., Hasselmann, K., 1984. On the existence of a fully developed wind-sea spectrum. *J. Phys. Oceanogr.* 14 (8), 1271–1285.
- Kumar, N., Voulgaris, G., Warner, J., Olabarrieta, M., 2012. Implementation of the vortex force formalism in the coupled ocean-atmosphere-wave-sediment transport (COAWST) modeling system for inner shelf and surf zone applications. *Ocean Modelling.* 47, Elsevier, pp. 65–95.
- McWilliams, J., Restrepo, J., Lane, E., 2004. An asymptotic theory for the interaction of waves and currents in coastal waters. *J. Fluid Mech.* 511, 135–178.
- McWilliams, J.C., Sullivan, P.P., Moeng, C.H., 1997. Langmuir turbulence in the ocean. *J. Fluid Mech.* 334, 1–30.
- Mellor, G., 2003. The three-dimensional current and surface wave equations. *J. Phys. Oceanogr.* 33, 1978–1989.
- Mellor, G., 2015. A Combined Derivation of the Integrated and Vertically Resolved, Coupled Wave-Current Equations. *J. Phys. Oceanogr.* 45. American Meteorological Society, pp. 1453–1463.
- Mellor, G.L., Yamada, T., 1982. Development of a turbulence closure model for geophysical fluid problems. *Rev. Geophys. Space Phys.* 20, 851–875.
- Melville, W., Rapp, R.J., 1985. Momentum flux in breaking waves. *Nature* 317 (6037), 514–516.
- Moghimi, S., Klingbeil, K., Grwe, U., Burchard, H., 2013. A direct comparison of a depth-dependent radiation stress formulation and a vortex force formulation within a three-dimensional coastal ocean model. *Ocean Modell.* 70, 132–144.
- Mulligan, R., Bowen, A., Hay, A., Van der Westhuysen, A., Battjes, J., 2008. Whitecapping and wave field evolution in a coastal bay. *J. Geophys. Res.* 113 (C3), C03008.
- Newberger, P., Allen, J., 2007. Forcing a three-dimensional, hydrostatic, primitive-equation model for application in the surf zone: 2. Application to duck94. *J. Geophys. Res.* 112 (C8), C08019.
- Plant, W.J., 1982. A relationship between wind stress and wave slope. *J. Geophys. Res.* 87 (C3), 1961–1967.
- Rasche, N., Chapron, B., Arduhin, F., Soloviev, A., 2013. A note on the direct injection of turbulence by breaking waves. *Ocean Modell.* 70, 145–151.
- Ruessink, B., Miles, J., Feddersen, F., Guza, R., Elgar, S., 2001. Modeling the alongshore current on barred beaches. *J. Geophys. Res.* 106 (C10), 22451–22464.
- Shchepetkin, A., McWilliams, J., 2005. The regional oceanic modeling system (ROMS): a split-explicit, free-surface, topography-following-coordinate oceanic model. *Ocean Modell.* 9, 347–404.
- Shchepetkin, A.F., McWilliams, J.C., 2003. A method for computing horizontal pressure-gradient force in an oceanic model with a nonaligned vertical coordinate. *J. Geophys. Res.* 108, 1–34. doi:10.1029/2001JC001047.
- Snyder, R., Elliott, J., 1981. Array measurements of atmospheric pressure fluctuations above surface gravity waves. *J. Fluid Mech.* 102 (1), 1–59.
- Soloviev, A., Lukas, R., 2003. Observation of wave-enhanced turbulence in the near-surface layer of the ocean during toga coare. *Deep Sea Res. Part I: Oceanogr. Res. Pap.* 50 (3), 371–395.
- Stewart, R., Grant, H.L., 1962. Determination of the rate of dissipation of turbulent energy near the sea surface in the presence of waves. *J. Geophys. Res.* 67 (8), 3177–3180.
- Stips, A., Burchard, H., Bolding, K., Prandke, H., Simon, A., Wuest, A., 2005. Measurement and simulation of viscous dissipation in the wave affected surface layer. *Deep Sea Res. Part II: Top. Stud. Oceanogr.* 52, 1133–1155.
- Tang, C., Perrie, W., Jenkins, A., DeTracey, B., Hu, Y., Toulany, B., Smith, P., 2007. Observation and modeling of surface currents on the grand banks: a study of the wave effects on surface currents. *J. Geophys. Res.: Oceans* 112 (C10), 1978–2012.
- Terray, E.A., Donelan, M.A., Agrawal, Y.C., Drennan, W.M., Kahma, K.K., Williams III, A.J., Hwang, P.A., Kitaigorodskii, S.A., 1996. Estimates of kinetic energy dissipation under breaking waves. *J. Phys. Oceanogr.* 26, 792–807.
- Terray, E.A., Drennan, W.M., Donelan, M.A., 1999. The vertical structure of shear and dissipation in the ocean surface layer. In: Banner, M.L. (Ed.), *The Wind-Driven Air–Sea Interface. Electromagnetic and Acoustic Sensing, Wave Dynamics and Turbulent Fluxes*. School of Mathematics, University of NSW, Australia, pp. 239–245.
- Thomson, J., 2012. Wave breaking dissipation observed with SWIFT drifters. *J. Atmos. Ocean. Technol.* 29 (12), 1866–1882.
- Thomson, J., Horner-Devine, A.R., Zippel, S., Rusch, C., Geyer, W., 2014. Wave breaking turbulence at the offshore front of the Columbia river Plume. *Geophys. Res. Lett.* 41 (24), 8987–8993.
- Thorpe, S.A., 1984. On the determination of K_r in the near-surface ocean from acoustic measurements of bubbles. *J. Phys. Oceanogr.* 14, 855–863.

- Uchiyama, Y., McWilliams, J., Shchepetkin, A., 2010. Wave–current interaction in an oceanic circulation model with a vortex-force formalism: application to the surf zone. *Ocean Modell.* 34, 16–35.
- Umlauf, L., Burchard, H., 2003. A generic length-scale equation for geophysical turbulence model. *J. Mar. Res.* 61 (2), 235–265.
- Umlauf, L., Burchard, H., Bolding, K., 2005. The general ocean turbulence model (GOTM) scientific documentation. Version 3.2. Technical Report 63. Leibniz-Institute for Baltic Sea Research, Warnemünde, Germany.
- Umlauf, L., Burchard, H., Hutter, K., 2003. Extending the $k-\omega$ turbulence model towards oceanic applications. *Ocean Modell.* 5, 195–218.
- van der Westhuysen, A.J., Zijlema, M., Battjes, J.A., 2007. Nonlinear saturation-based whitecapping dissipation in swan for deep and shallow water. *Coast. Eng.* 54 (2), 151–170.
- Wargula, A., Raubenheimer, B., Elgar, S., 2014. Wave-driven along-channel subtidal flows in a well-mixed ocean inlet. *J. Geophys. Res.* 119 (5), 2987–3001.
- Wilcox, D.C., 1988. Reassessment of the scale-determining equation for advanced turbulence models. *AIAA J.* 26 (11), 1299–1310.
- Willmott, C.J., 1982. Some comments on the evaluation of model performance. *Bull. Am. Meteorol. Soc.* 63 (11), 1309–1313.
- Yan, L., 1987. An improved wind input source term for third generation ocean wave modelling. Technical Report. Koninklijk Nederlands Meteorologisch Instituut.
- Zippel, S., Thomson, J., 2015. Wave breaking and turbulence at a tidal inlet. *J. Geophys. Res.: Oceans* 120 (2), 1016–1031.